

Structural stability and ion migration of Li_2MnO_3 cathode material under high pressures

Ze-Ren Xie(谢泽仁), Si-Si Zhou(周思思), Bei-Bei He(贺贝贝), Huan-Wen Wang(王欢文), Yan-Sheng Gong(公衍生), Jun Jin(金俊), Xiang-Gong Zhang(张祥功), and Rui Wang(汪锐)

Citation: Chin. Phys. B, 2023, 32 (**12**): 126101. DOI: 10.1088/1674-1056/ace2b1

Journal homepage: http://cpb.iphy.ac.cn; http://iopscience.iop.org/cpb

What follows is a list of articles you may be interested in

Prediction of superionic state in LiH_2 at conditions enroute to nuclear fusion

Fude Li(李福德), Hao Wang(王豪), Jinlong Li(李津龙), and Huayun Geng(耿华运)

Chin. Phys. B, 2023, 32 (**10**): 106103. DOI: 10.1088/1674-1056/acea68

Pressure-induced stable structures and physical properties of Sr-Ge system

Shuai Han(韩帅), Shuai Duan(段帅), Yun-Xian Liu(刘云仙), Chao Wang(王超), Xin Chen(陈欣), Hai-Rui Sun(孙海瑞), and Xiao-Bing Liu(刘晓兵)

Chin. Phys. B, 2023, 32 (**1**): 016101. DOI: 10.1088/1674-1056/ac6db5

Structural evolution and molecular dissociation of H_2S under high pressures

Wen-Ji Shen(沈文吉), Tian-Xiao Liang(梁天笑), Zhao Liu(刘召), Xin Wang(王鑫), De-Fang Duan(段德芳), Hong-Yu Yu(于洪雨), and Tian Cui(崔田)

Chin. Phys. B, 2022, 31 (**7**): 076102. DOI: 10.1088/1674-1056/ac5980

Structural evolution and bandgap modulation of layered β-$GeSe_2$ single crystal under high pressure

Hengli Xie(谢恒立), Jiaxiang Wang(王家祥), Lingrui Wang(王玲瑞), Yong Yan(闫勇), Juan Guo(郭娟), Qilong Gao(高其龙), Mingju Chao(晁明举), Erjun Liang(梁二军), and Xiao Ren(任霄)

Chin. Phys. B, 2022, 31 (**7**): 076101. DOI: 10.1088/1674-1056/ac6db8

Raman spectroscopy investigation on the pressure-induced structural and magnetic phase transition in two-dimensional antiferromagnet $FePS_3$

Hong Zeng(曾鸿), Tingting Ye(叶婷婷), Peng Cheng(程鹏), Deyuan Yao(姚德元), and Junfeng Ding(丁俊峰)

Chin. Phys. B, 2022, 31 (**5**): 056109. DOI: 10.1088/1674-1056/ac5a41

Structural stability and ion migration of Li_2MnO_3 cathode material under high pressures

Ze-Ren Xie(谢泽仁)[1], Si-Si Zhou(周思思)[2], Bei-Bei He(贺贝贝)[1], Huan-Wen Wang(王欢文)[1], Yan-Sheng Gong(公衍生)[1], Jun Jin(金俊)[1], Xiang-Gong Zhang(张祥功)[2], and Rui Wang(汪锐)[1,†]

[1] *Faculty of Materials Science and Chemistry, China University of Geosciences, Wuhan* 430074, *China*
[2] *Wuhan Institute of Marine Electric Propulsion, Wuhan* 430064, *China*

(Received 13 April 2023; revised manuscript received 16 June 2023; accepted manuscript online 29 June 2023)

Some special fields, such as deep-sea exploration, require batteries and their electrode materials to withstand extremely high pressure. As the cathode material has the highest energy density, Li-excess Mn-based materials are also likely to be utilized in such an environment. However, the effect of pressure on the crystal structure and migration barrier of this kind of material is still not clear at present. Therefore, in this study, we investigate the properties of the matrix material of Li-excess Mn-based material, Li_2MnO_3, under high pressure. The equation of state, bulk modulus, and steady-state volume of Li_2MnO_3 are predicted by the method of first principles calculation. The calculations of unit cells at different pressures reveal that the cell parameters suffer anisotropic compression under high pressure. During compression, Li–O bond is more easily compressed than Mn–O bond. The results from the climbing image nudged elastic band (CINEB) method show that the energy barrier of Li^+ migration in the lithium layer increases with pressure increasing. Our study can provide useful information for utilizing Li-excess Mn-based materials under high pressure.

Keywords: lithium-ion battery, Li_2MnO_3, high pressure, DFT computation

PACS: 61.50.–f, 82.47.Aa, 91.60.Gf, 31.15.–p **DOI:** 10.1088/1674-1056/ace2b1

1. Introduction

The ocean covers 70% of the Earth's surface, and areas deeper than 10^3 meters occupy more than 90% of the overall ocean area. The deep sea contains abundant oil, gas resources, and mineral resources. In order to develop these resources, new types of diving technology and equipment are required to meet the demands of deep-sea resource exploration.[1,2] In 2020, China sent a manned submersible, named "Striver", into Earth's deepest ocean trench. Lithium-ion batteries were chosen and used because of their high energy density, low self-discharge, and long life.[3–8] When used under such a condition, the electrode materials in the battery also experience enormous pressure.[9–12] Therefore, the properties of cathode materials under high pressure are worth studying. So far, the characteristics of $LiCoO_2$,[13] $LiFePO_4$,[14] and $Li[Li_{1/3}Ti_{5/3}]O_4$[15] under high pressures have been studied.

However, as the material with the highest energy density, the structural evolution and migration energy barrier of Li-excess Mn-based materials under high pressures are not yet clear.[16–19] The Li-excess Mn-based materials can be denoted as $xLi_2MnO_3(1-x)LiMnO_2$ $(0 < x \leq 1)$, where M is typically Mn, Ni, and Co.[20,21] This kind of material has advantages of high energy density, low cost, and high voltage, but their rapid capacity decline and low coulomb efficiency and other problems hinder its commercial applications.[22–24] The Li_2MnO_3 (LMO) is believed to be the matrix material of Li-excess Mn-based materials.[25,26] As the key component, LMO can not only store lithium between layers, but also enhance the structural stability of layered Li-rich oxides.[27] Therefore, the study of LMO can provide ideas for solving the problems of structural stability, lattice oxygen loss, and capacity attenuation of layered lithium–oxide materials.

In this work, the equation of state, bulk modulus, steady-state volume, and migration energy barrier of LMO under high pressures are studied. It is reported that LMO still maintains a monoclinic phase at 12 GPa.[28] To avoid phase transition caused by pressure,[29] 12 GPa was taken as the upper limit in this research.

2. Method

In this work, the Vienna *ab initio* simulation package (VASP[30]) was used for spin-polarized density functional theory (DFT) calculations. The exchange–correlation function uses the Perdewe–Burkee–Ernzerhof (PBE) functional, and the electron–ion interaction is represented by the projector augmented wave (PAW) method. Considering the existence of strongly correlated electrons of Mn in Li_2MnO_3 electrode materials, the method of GGA+U ($U = 3.9$)[31,32] was used. In all calculations, the wave function had a plane wave cutoff energy of 600 eV. This set of parameters could make the residual stress between atoms in the optimized unit cell less than 0.01 eV·Å^{-1}, and the total energy convergence threshold did not exceed 10^{-5} eV. Relaxed structure calculations were performed at different constant volumes and the energy–volume

†Corresponding author. E-mail: wangrui@cug.edu.cn
© 2023 Chinese Physical Society and IOP Publishing Ltd

data were fitted to a third-order Birch–Murnaghan equation of state (EOS):[33]

$$E(V) = E_0 + \frac{9V_0B_0}{16}\left\{\left[\left(\frac{V_0}{V}\right)^{2/3}-1\right]^3 B_0' + \left[\left(\frac{V_0}{V}\right)^{2/3}-1\right]^2\left[6-4\left(\frac{V_0}{V}\right)^{2/3}\right]\right\}, \quad (1)$$

$$P(V) = \frac{3B_0}{2}\left[\left(\frac{V_0}{V}\right)^{7/3}-\left(\frac{V_0}{V}\right)^{5/3}\right] \times\left\{1+\frac{3}{4}(B_0'-4)\left[\left(\frac{V_0}{V}\right)^{2/3}-1\right]\right\}. \quad (2)$$

The equation of state is a description of the P–V state relationship of a solid at constant temperature. The E–V equation (formula (1)) and P–V equation (formula (2)) have the same four parameters, *i.e.*, E_0 (steady-state energy), V_0 (steady-state volume), B_0 (bulk elastic modulus), and B_1' (first-order differential of elastic modulus to volume). By fitting the E–V equation of the LMO, the relevant fitting parameters could be obtained to obtain the P–V equation. The migration energy barriers of lithium ions in $2\times2\times1$ supercell (96 atoms in total) were calculated by using the CINEB method, and the minimum energy for lithium-ion diffusion was obtained. Seven images were placed between the starting position and the ending position to simulate the process of lithium-ion migration.

3. Results and discussion

3.1. Structural stability of Li_2MnO_3 under high pressures

The calculation reproduces the monoclinic structure of the LMO (space group $C2/m$), and the calculation method of LDA+U is used to optimize the structure for comparisons. The cell parameter values and experimental values[34] of all optimized structures are shown in Table 1. The calculation results show that the cell parameter values obtained by using the GGA+U calculation method are close to the experimental values, and the same as other research results.[35,36]

Table 1. Calculated and measured values of LMO cell parameters.

	a (Å)	b (Å)	c (Å)
Exp.	4.937	8.532	5.030
LDA+U	4.855	8.397	4.906
GGA+U	4.992	8.627	5.065

The cell with optimized structure is adopted for calculation, and the third-order Birch–Murnaghan equation of state is used to fit the energy–volume diagram of the LMO as shown in Fig. 1(a). According to the fitting results, the bulk modulus of LMO is 109.1 GPa and its first derivative is 4.9. At zero pressure, the equilibrium volume of the LMO is 206.46 Å^3. The pressure–volume relation of LMO within 12 GPa is shown in Fig. 1(b). The prediction shows that at 12 GPa, the volume of LMO cell is about 189.5 Å^3, and the volume is compressed by about 8%, indicating that LMO is sensitive to high pressure environment.

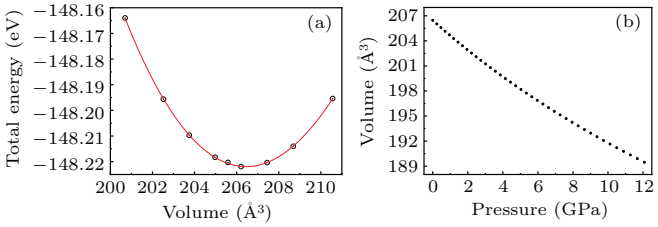


Fig. 1. (a) The energy–volume relation and (b) pressure–volume relation calculated by LMO based on the third-order Birch–Murnaghan equation of state.

The research results in Ref. [12] show that the LMO structure is still stable at 12 GPa under experimental conditions. Therefore, we performed phonon calculation for verification, and the results are shown in Fig. 2. There is no imaginary frequency in the phonon spectrum calculated under each pressure, which indicates that the atomic vibration is stable under the corresponding pressures.

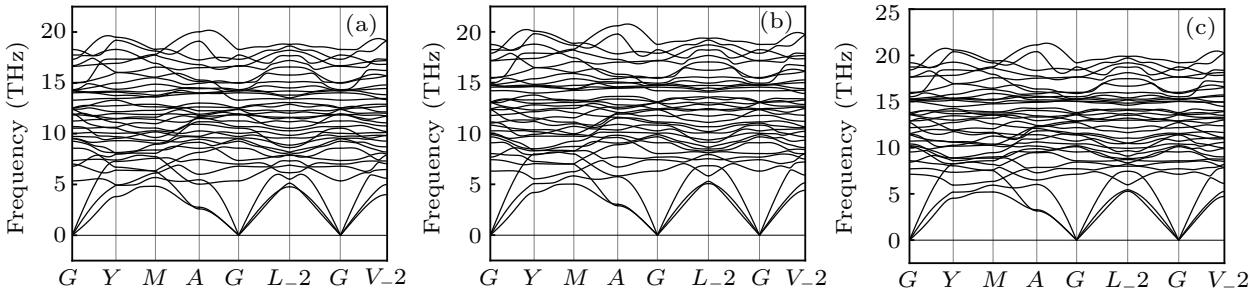


Fig. 2. Orbital overlap Hamiltonian population between Mn–O in LMO at 0 GPa (a), 4 GPa (b), and 8 GPa (c).

3.2. Anisotropic compressibility of Li_2MnO_3 under high-pressures

Figure 3(a) shows the variations of LMO cell parameters a, b, and c with pressures. The results show that the lattice parameters decrease with pressure increasing. At 12 GPa, lattice parameters are 4.862 Å, 8.410 Å, and 4.876 Å, respectively. After normalization, lattice parameters are reduced by 2.59%, 2.55%, and 3.72%. The compression rate of the cell is almost the same in the direction of [100] and [010], so it can be considered that the compression of the LMO in the di-

rection of [100] and [010] are isotropic under high pressures. However, the compression ratio in the direction of [001] is significantly higher than the two pressures above: about 1.45 times the compression ratio in the direction of [010], which shows anisotropic compression. According to the LMO structure (Fig. 3(b)), the layered structure of LMO in the direction [001] leads to large compressible space between layers.

To further study the compression mechanism of LMO under high pressures, the compression of chemical bonds and polyhedra in the cell are compared. Figure 3(c) shows that Li–O bond is compressed by 3.03% at 12 GPa, while Mn–O bond is compressed by only 1.58%. Similarly, figure 3(d) shows the volume compression ratio of the polyhedron LiO_6 (8.74%) is significantly higher than that of MnO_6 (4.31%). Obviously, the calculation results indicate that the Li–O bond is easier to compress than the Mn–O bond, resulting in stronger compressibility of the octahedron LiO_6, and the compression ratio in the direction of cell [001] is different from that in the direction of [100] and [010]. Like the research results in Ref. [37], the higher the pressure, the more serious the deformation is. The migration of transition metal manganese ions to the lithium layer may also be related to the inconsistent compression ratio of the polyhedron.

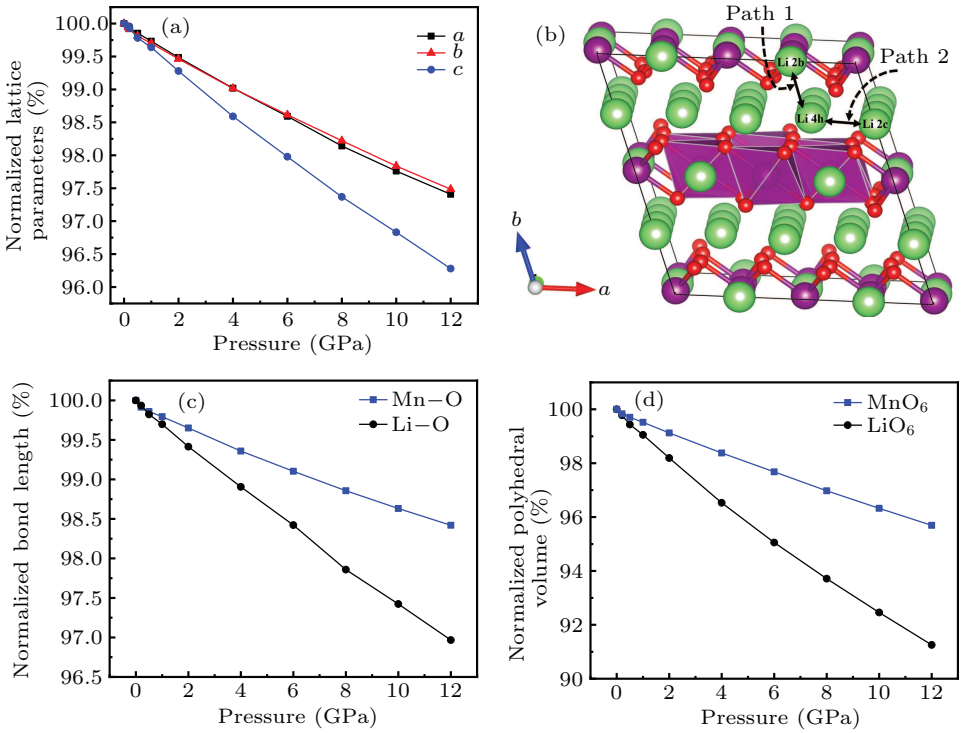


Fig. 3. (a) Influence of pressure on LMO cell parameters, (b) LMO cell structure, (c) normalized bond length change of Li–O and Mn–O bonds with pressures, and (d) normalized volume of polyhedral LiO_6 and MnO_6 *versus* pressures.

3.3. Electronic structure of Li_2MnO_3 under high-pressures

Figure 4 shows the calculated electronic structures of LMO under different pressures. When the pressures are 0 GPa, 4 GPa, and 8 GPa, the band gaps are 1.734 eV, 1.799 eV, and 1.986 eV, respectively. When the pressure is 0 GPa, the calculated band gap is consistent with related research result,[38,39] and with the gradual increase of pressure, the band gap begins to expand. This means that it is harder for electrons in the occupied state to transition to the unoccupied state, and the electrical conductivity of the electrons will gradually decrease. This can regulate the electrical properties of the material.

In order to better expound the influence of pressure on the stability of the cell in terms of electronic structure, we calculate the projected crystal orbital Hamilton populations (pCOHPs) of Mn and O atoms under different pressures, and the results are shown in Fig. 5. Figures 5(a)–5(c) show the –pCOHP graphs of LMO under 0 GPa, 4 GPa, and 8 GPa, respectively. The integral of pCOHP (IpCOHP) is used to determine the influence of pressure on the stability of Mn–O bond. According to Fig. 5(a), it can be found that at 0 GPa, there are some anti-bonding components in a range from −1.8 eV to 0 eV, and below −1.8 eV, bonding components are the main components. At this time, the stability of Mn–O bond is mainly contributed by bonding electrons. However, at 4 GPa and 8 GPa, it can be seen from the –pCOHP diagram that there are a large number of anti-bonding electrons below the fermi level, which reduces the stability of Mn–O bond. This is also illustrated in IpCOHP. The IpCOHP values at 0 GPa, 4 GPa, and 8 GPa are −2.12, −0.73, and −0.57, respectively, showing a gradually increasing trend. Therefore, pressure can affect the stability of Mn–O chemical bond in LMO cells to a certain extent.

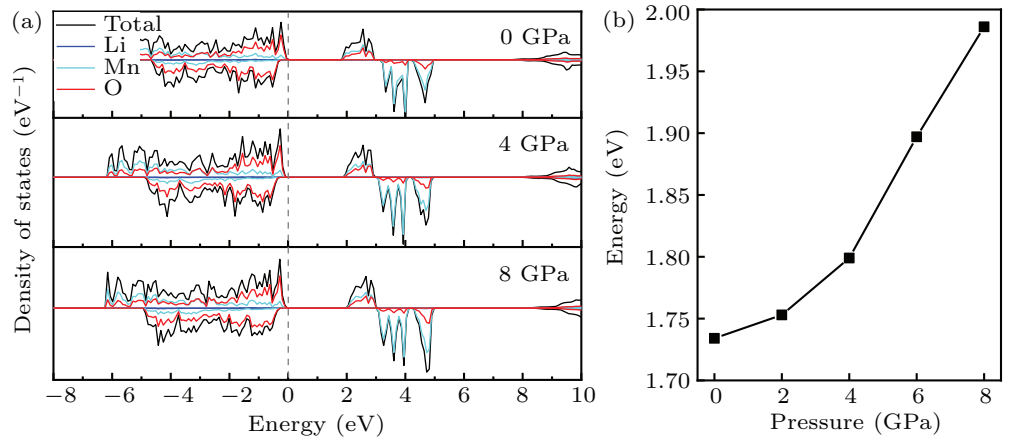


Fig. 4. LMO electronic structure changing with energy at 0 GPa, 4 GPa, and 8 GPa, respectively.

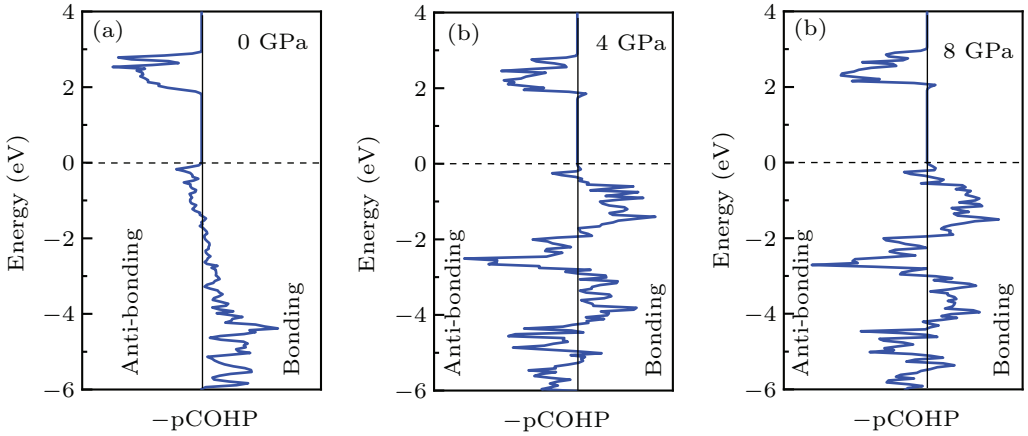


Fig. 5. pCOHP between Mn atom and O atom at 0 GPa (a), 4 GPa (b), and 8 GPa (c), respectively.

3.4. Li-ion migration barrier energy of Li_2MnO_3 under high-pressures

The CINEB method is used to calculate the migration path and migration energy barrier of Li^+ in LMO under high-pressure compression,[40] and the ion migration paths are shown in Fig. 3(b), where path 1 represents the migration of Li^+ at Wyckoff position 4*h*[41] in the lithium layers to site 2*b* in the transition metal layers, and path 2 represents the migration of Li^+ at site 4*h* in the lithium layer to site 2*c* in the lithium layer. At 0 GPa, the migration energy barrier of path 1 and path 2 are 0.589 eV and 0.499 eV, respectively, as shown in Fig. 6(a). The calculation of the path 2 energy barrier is almost consistent with the related literature reports. The calculation results show that the Li^+ migration energy barrier height of path 1 is about 0.09 eV higher than that of path 2. Figure 6(a) also shows that the energy of Li^+ at site 2*b* is very higher than that at site 2*c*. This study indicates the huge difference in energy between the two paths from the perspective of energy, and Li^+ in the lithium layer is more prone to delithium.

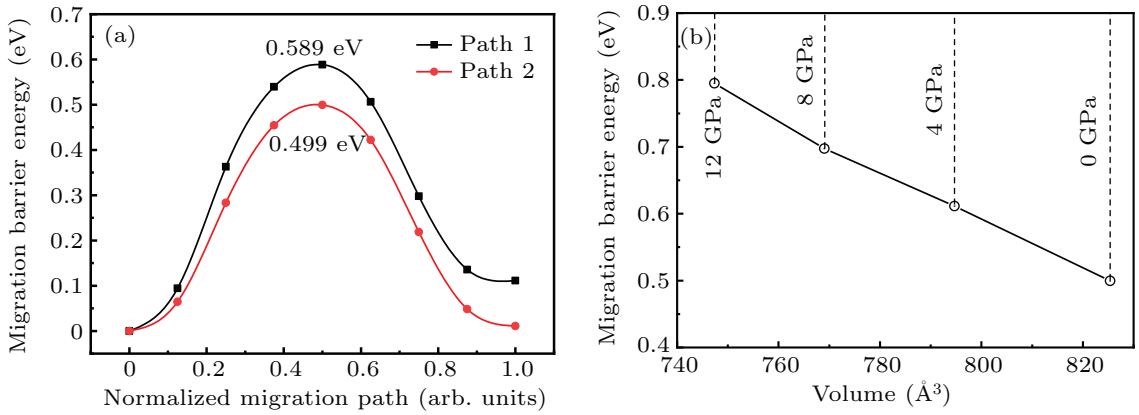


Fig. 6. Migration barriers of different paths at 0 GPa (a) and (b) calculated variations of Li^+ migration barrier energy with volume of path 2 under different pressures.

Based on the calculation of diffusion path 2, we studied the influence of pressure on the diffusion energy barrier. The migration energy barrier of Li^+ increases from about 0.499 eV at 0 GPa (825.38 Å^3 in volume) to nearly 0.795 eV at 12 GPa (747.37 Å^3 in volume), and the change process is almost linear. This indicates that under the condition of cell compression, the ion migration channel will limit the migration of Li^+, thus leading the ion conductivity to decrease. The decrease of ionic conductivity at high pressure makes LMO unsuitable as energy device for exploration in high-pressure environment such as deep sea or deep ground.

4. Conclusions

The structural stability and electrical conductivity of Li_2MnO_3 under high pressures are studied theoretically by using the first-principles calculations. The results show that the bulk modulus of the LMO is 109.1 GPa and the equilibrium volume is 206.46 Å^3. Under the same pressure, the compression rate of lattice parameters in the direction [100] and [010] are almost the same, but the compression rate of cell parameters in the direction [001] is obviously larger. The Li–O bond is more easily compressed than the Mn–O bond. The Li^+ at the 4*h* site in the lithium layer at 12 GPa is more likely to migrate to the 2*c* site in the same lithium layer, and the diffusion energy barrier increases almost linearly with the increase of the pressure. These research deepens our understanding of the structural and electrical properties of layered Li-excess Li_2MnO_3 under high pressures and can help us predict the effect of high voltage modification, which will provide useful information about the structural stability and conductive properties of cathode materials in the high pressure environment.

Acknowledgement

Project supported by the Research on High Power Flexible Battery in All Sea Depth, China (Grant No. 2020-XXXX-XX-246-00).

References

[1] Li G, Chen X, Zhou F, Liang Y, Xiao Y, Cao X, Zhang Z, Zhang M, Wu B, Yin S, Xu Y, Fan H, Chen Z, Song W, Yang W, Pan B, Hou J, Zou W, He S, Yang X, Mao G, Jia Z, Zhou H, Li T, Qu S, Xu Z, Huang Z, Luo Y, Xie T, Gu J, Zhu S and Yang W 2021 *Nature* **591** 66
[2] Hein J R, Koschinsky A and Kuhn T 2020 *Nature Reviews Earth & Environment* **1** 158–169
[3] Huang Y, Liu L and Gao M 2020 *Solid State Ionics* **346** 115195
[4] Longo R C, Kong F T, Kc S, Park M S, Yoon J, Yeon D H, Park J H, Doo S G and Cho K 2014 *Phys. Chem. Chem. Phys.* **16** 11233
[5] Xu J, Zhang J, Pollard T P, Li Q, Tan S, Hou S, Wan H, Chen F, He H, Hu E, Xu K, Yang X Q, Borodin O and Wang C 2023 *Nature* **614** 694
[6] Cabana J, Kwon B J and Hu L 2018 *Acc. Chem. Res.* **51** 299
[7] Zhao X and Ceder G 2022 *Joule* **6** 2683
[8] Wen G, Tan L, Lan X, Zhang H, Hu R, Yuan B, Liu J and Zhu M 2021 *Sci. China Mater.* **64** 2683
[9] Bandiello E, Errandonea D, Pellicer-Porres J, Garg A B, Rodriguez-Hernandez P, Munoz A, Martinez-Garcia D, Rao R and Popescu C 2018 *Inorg. Chem.* **57** 10265
[10] Lethole N L, Chauke H R and Ngoepe P E 2019 *Comput. Theor. Chem.* **1155** 67
[11] Dong H, Guo H, He Y, Gao J, Han W, Lu X, Yan S, Yang K, Li H, Chen D and Li H 2017 *Solid State Ionics* **301** 133
[12] Zhang X, Wang M, Wang Y, Zhou S, Yang G, Ren Y, Wang Q, Zhang R, Zheng J, Lu X, Yang W and Chen L 2021 *Solid State Ionics* **364** 115637
[13] Wang S, Liu J, Qie Y, Gong S, Sun Q and Jena P 2018 *J. Mater. Chem. A* **6** 18449
[14] Ashton T E, Laveda J V, MacLaren D A, Baker P J, Porch A, Jones M O and Corr S A 2014 *J. Mater. Chem. A* **2** 6238
[15] Mukai K and Yamada I 2018 *Inorganic Chemistry Frontiers* **5** 1941
[16] Vinckeviciute J, Kitchaev D A and Van der Ven A 2021 *Chem. Mater.* **33** 1625
[17] Hu W, Wang H, Luo W, Xu B and Ouyang C 2020 *Solid State Ionics* **347** 115257
[18] Wang S, Liu J and Sun Q 2017 *J. Mater. Chem. A* **5** 16936
[19] Zhuo Z, Dai K, Qiao R, Wang R, Wu J, Liu Y, Peng J, Chen L, Chuang Y D, Pan F, Shen Z X, Liu G, Li H, Devereaux T P and Yang W 2021 *Joule* **5** 975
[20] Nayak P K, Erickson E M, Schipper F, Penki T R, Munichandraiah N, Adelhelm P, Sclar H, Amalraj F, Markovsky B and Aurbach D 2018 *Adv. Energy Mater.* **8** 1702397
[21] Zhan C, Cai F, Amine K and Lu J 2017 *ACS Energy Lett.* **2** 1628
[22] Li X, Li X, Monluc L, Chen B, Tang M, Chien P H, Feng X, Hung I, Gan Z, Urban A and Hu Y Y 2022 *Adv. Energy Mater.* **12** 2200427
[23] Wang C, Yang C and Zheng Z 2022 *Adv. Sci.* **9** 2105213
[24] He W, Guo W, Wu H, Lin L, Liu Q, Han X, Xie Q, Liu P, Zheng H, Wang L, Yu X and Peng D L 2021 *Adv. Mater.* **33** 2005937
[25] Wang R, He X, He L, Wang F, Xiao R, Gu L, Li H and Chen L 2013 *Adv. Energy Mater.* **3** 1358
[26] He P, Yu H and Zhou H 2012 *J. Mater. Chem.* **22** 3680
[27] Li S, Fu X, Liang Y, Wang S, Zhou X a, Dong H, Tuo K, Gao C and Cui X 2020 *ACS Sustainable Chem. Eng.* **8** 9311
[28] Mukai K, Uyama T and Yamada I 2019 *ACS Omega* **4** 6459
[29] Cheng H, Li Y C, Li G and Li X D 2016 *Chin. Phys. Lett.* **33** 096104
[30] Kresse G and Joubert D 1999 *Phys. Rev. B* **59** 1758
[31] Anisimov V I, Zaanen J and Andersen O K 1991 *Phys. Rev. B* **44** 943
[32] Tamura T, Ohwaki T, Ito A, Ohsawa Y, Kobayashi R and Ogata S 2012 *Modelling and Simulation in Materials Science and Engineering* **20** 045006
[33] Oertel M, Hempel M, Klähn T and Typel S 2017 *Rev. Mod. Phys.* **89** 015007
[34] Boulineau A, Croguennec L, Delmas C and Weill F 2009 *Chem. Mater.* **21** 4216
[35] Chen H and Islam M S 2016 *Chem. Mater.* **28** 6656
[36] Pulido R, Naveas N, Martín-Palma J R, Graber T, Brito I, Hernández-Montelongo J and Manso Silván M 2022 *Chem. Eng. J.* **441** 136019
[37] Huang Y, He Y, Sheng H, Lu X, Dong H, Samanta S, Dong H, Li X, Kim D Y and Mao H K 2019 *Nat. Sci. Rev.* **6** 239
[38] Xiao R, Li H and Chen L 2012 *Chem. Mater.* **24** 4242
[39] Xie Z, Wu X, Zhang Y, Li G, Ma F, Yan W, Chen Y, Li F and Zhou M 2022 *Journal of Electroanalytical Chemistry* **922** 116762
[40] Jiang Y S, Yu F D, Que L F, Deng L, Xia Y, Ke W, Han Y and Wang Z B 2021 *ACS Energy Lett.* **6** 3836
[41] Serrano-Sevillano J, Carlier D, Saracibar A, Lopez del Amo J M and Casas-Cabanas M 2019 *Inorg. Chem.* **58** 8347